Chinese Journal of Aeronautics, (2024), 37(1): 162–172

Chinese Society of Aeronautics and Astronautics
& Beihang University

Chinese Journal of Aeronautics

cja@buaa.edu.cn
www.sciencedirect.com

Deployment analysis of composite thin-walled lenticular tubes with effect of storage time and temperature

Jinfeng DENG [a], **Ning AN** [a,b,c,*], **Qilong JIA** [b], **Xiaofei MA** [d]

[a] *School of Aeronautics and Astronautics, Sichuan University, Chengdu 610065, China*
[b] *State Key Laboratory for Strength and Vibration of Mechanical Structures, School of Aerospace, Xi'an Jiaotong University, Xi'an 710049, China*
[c] *State Key Laboratory of Structural Analysis for Industrial Equipment, Dalian University of Technology, Dalian 116024, China*
[d] *Xi'an Institute of Space Radio Technology, Xi'an 710100, China*

Received 2 November 2022; revised 15 November 2022; accepted 5 March 2023
Available online 13 May 2023

KEYWORDS

Composite deployable structures;
Deployment dynamics;
Finite element method;
Stress relaxation;
Thin-walled booms

Abstract Composite Thin-walled Lenticular Tube (CTLT) is increasingly utilized in small satellites missions as a lightweight, foldable, and rollable structural material that facilitates the construction of large deployable systems. The CTLT is initially flattened and coiled around a central hub for storage before launch, during which elastic energy is stored as deformation energy, allowing it to be self-deployed on demand for use in orbit. This work presents a comprehensive investigation into the coiling, storage and deployment behaviors of CTLT that wraps around a central hub. A nonlinear explicit dynamic finite element model was developed with both deformable CTLT and rigid-bodies mechanisms including the central hub and guide rollers, as well as the complex interactions among them. The coiling mechanics characteristics such as stored strain energy and rotational moment were presented and validated against experimental data in the literature. Then, the dynamic deployment behaviors were analyzed in terms of two different deployment methods, namely, controlled deployment and free deployment. The effect of material property change during storage was also discussed through numerical experiments.

1. Introduction

In recent years, Deployable Composite Booms (DCBs) have been attracting increasing attention in aerospace engineering due to their lightweight and compact nature, and potential applications in small satellites. The booms are usually fabricated as ultra-thin-walled tubular structures, which enables them to be easily flattened and rolled up into a small volume

* Corresponding author.
E-mail address: anning@scu.edu.cn (N. AN).
Peer review under responsibility of Editorial Committee of CJA.

Production and hosting by Elsevier

https://doi.org/10.1016/j.cja.2023.05.011

before and during launch, and capable of self-deploying for use in space. A wide range of small satellite deployable systems such as solar arrays, wrapped-rib antennas, drag sails, and solar sails have been demonstrated by using DCBs as supporting structures.[1–9] Composite Thin-walled Lenticular Tube (CTLT) is one of the popular types of DCBs which features a closed tubular structure made of two thin omega-shaped cylindrical shells jointed together to form a lenticular-shaped cross-section. Compared to the alternative types of DCBs with open cross-sections such as C-shaped tape springs, Storable Tubular Extensible Mast (STEM) booms, and Triangular Rollable And Collapsible (TRAC) booms, the lenticular-shaped cross-section provides the CTLT larger torsional stiffness[10] and better bending buckling resistance performance.[11] Very recent years have seen a few variations and extensions to conventional lenticular-shaped cross-sections of CTLTs to continuously increase efficiency, e.g., the four-cell lenticular honeycomb deployable boom,[12] and the corrugated rollable tubular boom.[13,14].

At the core of designing and implementing CTLTs is the need to quantify their coiling and deployment performance. Fig. 1 schematizes two different ways of realizing coiling and deployment for a CTLT. The first way involves flattening and attaching one end of CTLT to a central hub, and then using a hub motor to drive it. When the motor rotates anticlockwise, the CTLT is coiled, while a clockwise rotation causes it to deploy, see Fig. 1(a). This method produces a steady and controlled deformation process and is suitable for the deployment of large-scale solar sails. For example, in the SIASAIL-I solar sail design, four bistable tubular booms are initially fixed and coiled around a central hub. Deployment is then executed by slowly rotating the central hub, causing all the booms to be pushed out synchronously, which deploys the solar membrane for operation.[5] On the other hand, the deployment of CTLT could also be driven by the boom's stored strain energy instead of using a motor. As described in Fig. 1(b), one end of CTLT is flattened and attached to the central hub, but the hub is constrained from any rotation. The coiling is achieved by manually rotating the boom structure and the subsequent deployment is driven by releasing the stored strain energy, which is a truly dynamic transient process. One notable application of this uncontrolled free deployment manner is in the design of wrapped-rib space antenna.[15].

In the past few years, a number of studies have been conducted to assess the coiling and deployment mechanics characteristics of CTLTs.[16,17] An experimental testing platform[18,19] is usually comprised of a central driving roller, a few constraint shafts and guide plates, torque sensors, and some frame structures. These devices help control the coiling speed and allow users to measure the rotational moment as a function of coiling angle. Several analytical models have been formulated in addition to experiments based on the energy principle and classical laminate theory to predict the flattening force and rotational moment in the coiling process,[20] and numerical simulation provides an alternative approach to capture the contact interaction information between the deformable boom and surrounding rigid objects such as the central hub and guide rollers.[21] Numerical simulation also enables to capture the behavior of thin-walled composite deployable boom in a realistic manner, while providing details about stress redistribution and energy variation during the coiling and deployment process. It has been validated that the explicit dynamic finite element models generated using commercial codes (eg. ABAQUS, LS-DYNA) are capable of accurately predicting the mechanical characteristics of deployable composite booms in its process of flattening and coiling.[16,17,22,23] Besides, combining numerical simulation with optimization algorithms makes it possible to optimize the performance for CTLT designs.[24–26] However, most of the existing studies have been focused on the folding and coiling behaviors of CLTL, its deployment behavior remains largely uninvestigated.

A unique challenge in analyzing the deployment behavior of CTLT is the possible material property change during storage. Due to specific application scenarios in the outer space, CTLTs are often stored for several months or even years in the coiled state inside a spacecraft until deployment, while in the meantime being exposed to a severe thermal condition in the space environment.[6,27,28] Suffering from long-term stowage and severe temperature changes, CTLTs that are subjected to a constant strain may experience substantial material property change due to viscoelasticity of materials. The change in mate-

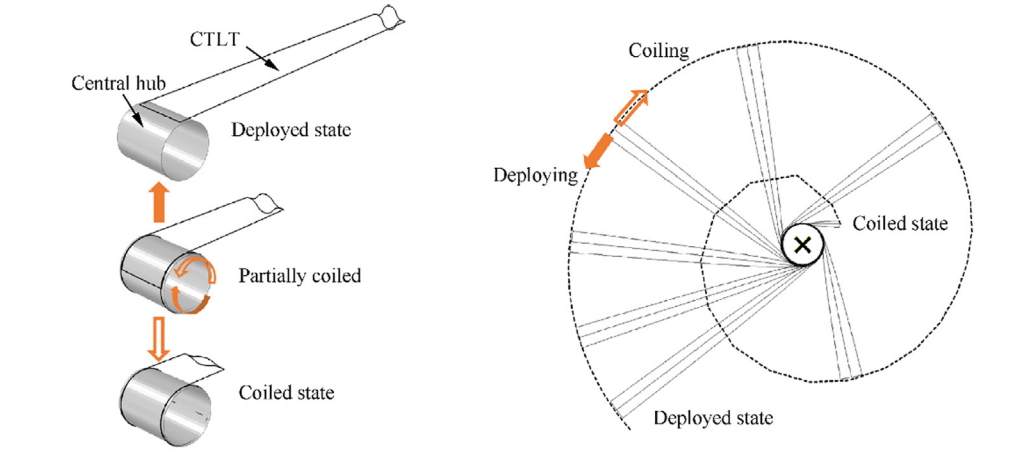

(a) In a controlled manner by slowly rotating the central hub

(b) In an uncontrolled manner by rotating the free end of CTLT along a helix trajectroy

Fig. 1 Two typical ways of realizing coiling and deployment for CTLT.

rial property will cause a change (increase or decrease) in the stored strain energy and ultimately produce an impact on the deployment performance. Adamcik et al.[29] performed an experimental study to investigate the impact of storage time and operation temperature on the deployment speed of CTLTs, and reported that the deployment performance of CTLTs degrades significantly as the storage time being longer or the operation temperature being higher. Kwok and Pellegrino[30] proposed a viscoelastic model that predicts the dynamic deployment behavior of single-ply plain-weave composite tape-spring shells that are deployed after being held folded for a given period of time. Long et al.[21,31] derived a linear anisotropic viscoelastic shell formulation and simulated the complete process of flattening, coiling, deployment and recovery of a CTLT boom structure.

The purpose of this study is to extend the research on previous coiling analysis of CTLT to a complete analysis covering coiling, storage, and deployment of CTLT. Specifically, we develop a generalized computational model for analyzing the coiling and dynamic deployment behavior of CTLT that wraps around a central hub, and we discuss the effect of storage on the deployment performance. The paper is focused on analysis of CTLT, but the method applies directly to any coilable booms. To facilitate future research and replication of our work, we have made the implementation of our model publicly available from https://github.com/SCU-An-group/coiling-deployment-CTLTs.

The content is organized as follows. Section 2 provides a detailed description of the computational model implementation. Section 3 presents the deformation behavior of CTLT during the quasi-static coiling process. The results were compared with experimental data in literature for validation. In Section 4, both quasi-static deployment behavior under controlled and transient dynamic deployment behavior in free deployment were simulated and analyzed. Then, the effect of storage was discussed in Section 5. Finally, concluding remarks are given in Section 6.

2. Finite element model

Fig. 2 illustrates the geometry and dimensions of CTLT, which has a lenticular cross-section consisting of two thin Ω-shaped shells of thickness t and longitudinal length l bonded together along the flat regions. Each Ω-shaped section is comprised of four circular arcs of radius r subtending an angle of 60°, and two straight segments called webs of width w. The values of the above-mentioned geometric parameters are listed in Table 1. Each Ω-shaped shell is made from a five-ply laminate of carbon fiber reinforced epoxy resin (T300/5228A) with a stacking sequence of [45/-45/0/-45/45]. Each lamina is transversely isotropic in the plane transverse to the fiber, and the five independent engineering constants are taken from[17] and summarized as following: $E_1 = 80.08\,\text{GPa}$, $E_2 = 6.67\,\text{GPa}$, $\nu_{12} = 0.34$, $G_{12} = 2.93\,\text{GPa}$, $G_{23} = 7.5\,\text{GPa}$, and the density of the laminate is 1.6 g/cm^3.

Table 1 Geometric parameters of CTLT.

Geometric parameter	Value
Longitudinal length l (mm)	1000
Web width w (mm)	10
Arc radius r (mm)	34
Shell thickness t (mm)	0.4

To capture the deformation of CTLT as well as the contact information between the CTLT and the central hub in the process of flattening, coiling and deployment, both the boom structure as well as the coiling/deployment mechanisms need to be modeled. The model was constructed by using the commercial finite element package ABAQUS 2020, and only one half of the geometry was created due to symmetry, see Fig. 3. The CTLT was modeled as a three-dimensional 3D deformable body using four-node reduced integration shell elements (ABAQUS element type S4R) with stiffness hourglass control. The coiling/deployment mechanisms are simplified as four components which are mandatory for reproducing the coiling and deployment process, including: (A) a central hub (light gray) with radius of 80 mm which is driven by electric motors for rotation and equipped with torque sensors to measure the rotational moment; (B) a group of 11 guide rollers (light blue) with the same radius of 5 mm, which are distributed equally along the circular path away from the hub surface at a gap distance of 2 mm. The guide rollers are used to maintain the coiled state of CTLT, and specifically, the roller No.1 (dark blue) and the central hub provide boundary conditions for the boom transition region; (C) a pair of flattening plates (dark gray) to compress the end of CTLT from its deployed state to the flattened state; and (D) a small constraint plate (orange) to clamp the flattened end of the CTLT to the

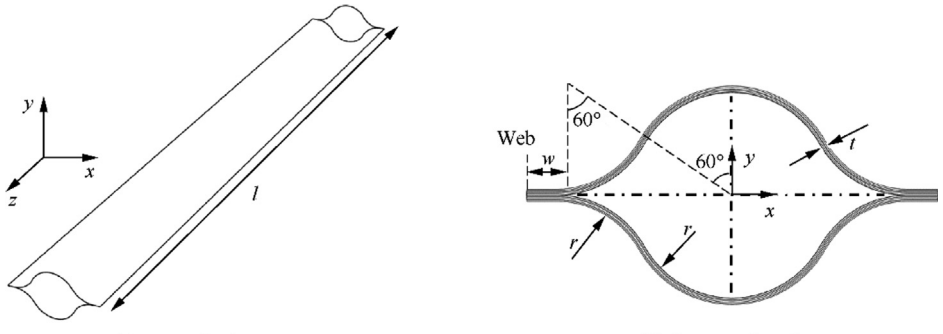

Fig. 2 Geometry of CTLT in its fully deployed state.

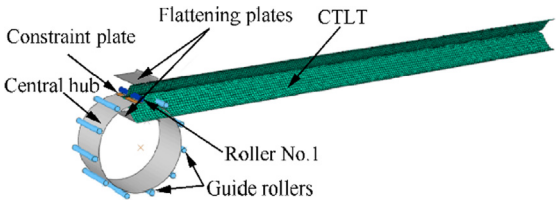

Fig. 3 Finite element model of CTLT and its coiling/deployment mechanism. CTLT is modeled as a deformable body with shell elements while the components of the coiling/deployment mechanism are modeled as rigid bodies. One half of the geometry was modeled due to symmetry.

central hub. The above-mentioned coiling/deployment mechanisms components have much larger modulus compared to the CTLT, and thus they were all modeled as rigid bodies using non-deformable shell elements (Abaqus element type R3D4). The simulations were performed by a dynamic explicit finite element procedure (*Dynamic, Explicit in ABAQUS). This type of analysis applies a central difference rule to explicitly integrate the equations of motion through time, requiring no iteration procedures and facilitating well-suited performance in solving dynamic process involved with significant geometry changes and complicated contact problems. Moreover, it has been proven valuable in solving quasistatic problems in terms of folding and deployment analysis of space deployable structures.[32–34].

The coiling and deployment process of CTLT could be modeled by the following steps:

Step 1. Compress one end of CTLT by moving the pair of flattening plates closer together to push the flattened end into the tiny gap between the constraint plate and the central hub. In this step only the contacts between the CTLT and the flattening plates were activated, and a friction contact with coefficient of friction 0.1 was assumed for tangential behavior.

Step 2. Deactivate the contacts between the CTLT and the flattening plates, and meanwhile create the contact between the CTLT and the constraint plate. The contact algorithm was defined with no slip and no separation conditions once the points are in contact. This contact constraint is similar to a tie constraint, which creates a bond between the flattened end of CTLT and the constraint plate. Besides, the contact between CTLT and the central hub as well as that between CTLT and guide rollers were also created in this step, where the interactions were modeled as a frictionless contact with separation allowed.

Step 3. Propagate the contact definition from the previous step, and apply a rotation of angle 10.5 radian (≈1.67 circles) around the hub axis to the central hub together with the constraint plate; the deployable CTLT would be progressively flattened and coiled into the gap between the central hub and guide rollers. Note that the rotation should be applied in a smooth manner under quasi-static conditions to exclude kinetic effects.

Step 4. The deployment could be accomplished either in a controlled quasi-static manner by reversely slowly rotating the central hub with all contact pairs retained, or on the other hand, in a free deployment dynamic manner by deactivating the contact constraints between the CTLT and guide rollers. Significant dynamic effects were expected to take place in the free deployment process, and an amount of damping was introduced in form of viscous pressure to damp out vibrations to avoid sudden failure of elements. The changes in contact definition with respect to simulation steps throughout the flattening, coiling and deployment process are concluded in Table 2.

The monitoring of the energy balance history provides the key test for the robustness of an explicit dynamic analysis. The energy balance, also referred to as total energy in ABAQUS, is defined as the difference between the energy stored in the structure and/or dissipated during the loading process and the work done by external forces. In all simulations presented in the manuscript, the total energy equation has the form as:

$$E_t = E_s + E_k - E_w \tag{1}$$

where E_t is the total energy, E_s is the strain energy, E_k is the kinetic energy, and E_w is the work done by external loads. The simulation accuracy can be assessed by means of two main checks on the energies.[23,32,34] First, the energy balance should remain zero, since in all the simulations the CTLT was deformed by an external work performed by the prescribed displacement and no other kinds of energy (e.g., thermal) was introduced. Second, to ensure a quasi-static condition, the kinetic energy should not exceed a small fraction (typically 2% to 5%) of the strain energy throughout the folding and coiling process.

3. Coiling behavior

To start with, the CTLT is flattened and coiled around the central hub, which allows it to be stowed thereafter and be deployed at the end. Elastic strain energy is stored in the deformation of CTLT in the flattening and coiling process. The energy variation results are given in Fig. 4. First of all, the stored strain energy gradually increases from 0-2.3 J as the end of CTLT is being flattened. Then, it remains almost unchanged in the new contact generation step because very little deformation is expected. Finally, the stored strain energy increases smoothly up to ~ 15.2 J in the coiling process. Fig. 4 also shows that the total energy of the model remains zero, and the kinetic energy is negligible compared to the strain energy throughout the flattening and coiling process; hence, the results are essentially quasi-static.

Fig. 5(a) plots the evolution of strain energy of CTLT E_s as a function of rotational angle θ of the central hub in the coiling process. The strain energy increases nearly linearly with the rotational angle. The rotational moment could be determined either by fitting the slope $M = dE_s/d\theta$ from the CTLT strain energy versus rotational angle curve, or by extracting the resultant moment acting on the central hub. Fig. 5(b) presents the evolution of rotational moment as a function of rotational angle results predicted by FEM against experimental data reported in literature.[17] FEM results are in fairly good agreement with experiments, demonstrating that the rotational moment increases with the increase of rotational angle within the initial small deformation range and reaches a stable level quickly. This means that the coiling deformation proceeds stably, again validating the quasi-static assumption in the coiling process. The discrepancy between simulation and experimental data may arise from the data scatter of torque measurement of

Table 2 Changes in contact definition with respect to simulation steps.

Contact pairs	Step 1. Flattening (Step time: 1 s)	Step 2. New contact (Step time: 0.5 s)	Step 3. Coiling (Step time: 2 s)	Step 4. Deployment (Controlled/Free) (Step time: 2 s)
CTLT - Flattening plates (friction, separation)	Created	Deactivated	Deactivated	Deactivated/Deactivated
CTLT - Constraint plates (no slip, no separation)	None	Created	Propagated	Propagated/Propagated
CTLT - Central hub (frictionless, separation)	None	Created	Propagated	Propagated/Propagated
CTLT - Guide rollers (frictionless, separation)	None	Created	Propagated	Propagated/ Deactivated

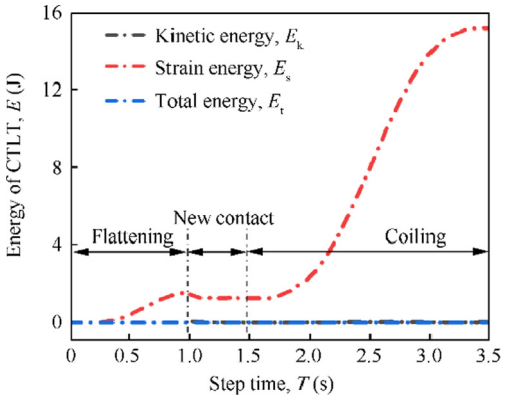

Fig. 4 Variation of strain energy of CTLT in the flattening and coiling process.

the central hub, especially when the boom is thin-walled and the rotation is dynamic. Because of the lack of details on the testing method, this discrepancy is understandable. Nevertheless, the whole story and the feasibility of the proposed numerical strategy do not change.

Fig. 6 presents the FEM deformation snapshots of stress distribution for the CTLT at various stages of the flattening and coiling process, which show that the highest stresses concentrate on the edges of the CTLT. The maximum stresses are much less than the strengths of the composite material, indicating that the CTLT was deformed without causing a failure of the structure. It should be noted that the CTLT design in this work is not intrinsically bistable.[35] Therefore, additional forces are required to help maintain the coiled state. These forces are provided by the normal contact forces between the guide rollers and the CTLT. Fig. 6(c) gives the contact force distribution at the 1.5 circle coiled state. Roller No.1 provides the maximum contact force among all the guide rollers because it works together with the central hub for realizing the boom cross-section transition from deployed to flattened state. To be specific, at the final coiled state of 1.5 circle, the normal contact force between the roller No.1 and the CTLT is about 100 N, compared to about 1 N between other rollers and the CTLT. It should be pointed out that similar results of the flattening and coiling process have been reported previously;[16,17,21] however, the simulations were performed for two purposes: (A) to validate the accuracy of our FEM model through a comparison to previously reported results; and (B) to store strain energy in the deformed CTLT and thus, make it ready for the subsequent deployment analysis.

4. Deployment behavior

This section presents the deployment analysis results. The two different ways of realizing the deployment of CTLT, i.e., the quasi-static controlled deployment as well as the true dynamic free deployment as discussed in Fig. 1, are both evaluated for making a comparison.

Fig. 7 illustrates the mechanical response of the CTLT in the controlled deployment process. The rotational angle was increased in a smooth manner to drive the rotation of the central hub, which controls the quasi-static deployment of the CTLT. Fig. 7(a) shows the rotational angle versus simulation step time. As the central hub is rotated, the CTLT boom is

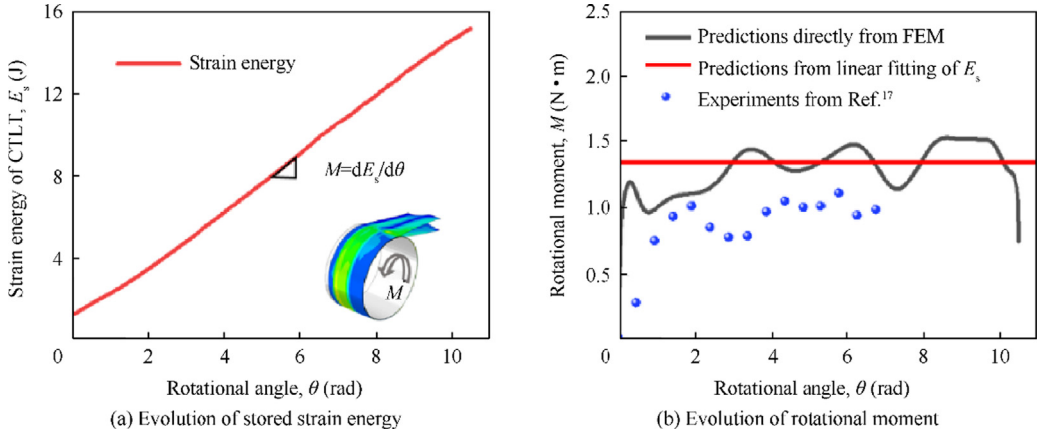

Fig. 5 Mechanical response of CTLT in quasi-static coiling process.

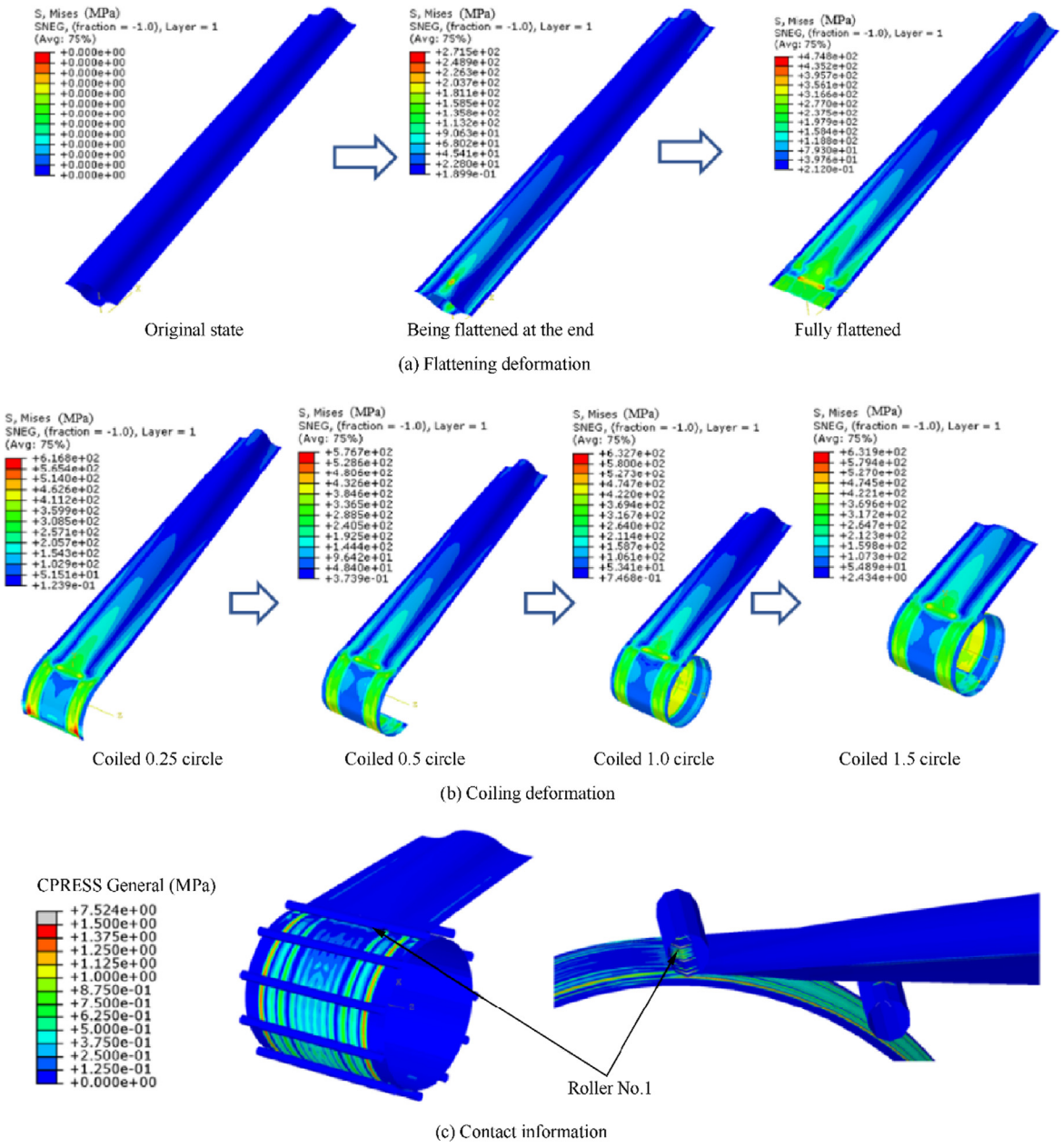

Fig. 6 FEM deformation snapshots of stress and contact pressure distribution for the CTLT at various stages in the flattening and coiling process.

deployed and its length increases. Meanwhile, the cross-section at the free end of the CTLT gradually opens up towards a lenticular shape. The recovery behavior of the CTLT could be quantified by calculating the shape recovery ratio φ of the deformed cross-section at the free end, with $\varphi = h/H$ being defined as the ratio between the current height of the shape h and the original height of the shape at stress-free state H. It is shown from Fig. 7(b) that the shape recovery ratio φ increases smoothly from $\sim$ 0.3 to a stable level of $\sim$ 1.2 as the step time increases. The final value of φ is greater than 1 because at the final deployed state the CTLT is not in its stress-free state (see Fig. 7(d)). Instead, one end of the CTLT is stilled flattened and attached on the central hub, and in this deformed state, the free end will be larger in height, which agrees with the findings of Wang et al.[36] Fig. 7(c) gives the evolution of the rotational moment as a function of step time. An interesting point we need to mention here is about the "blossoming" effect. Blossoming is a possible deployment failure mode of coiled thin-walled booms which is referred to as the phenomenon of stopping deployment and instead, unwinding and expanding within the deployment mechanism.[37–39] Literally, in our coiling and deployment simulation, we did not observe evident blossoming of the CTLT, and we attribute it to the relatively large amount of guide rollers and the tiny gap distance between the roller and central hub.

In contrast to the quasi-static behavior in the controlled deployment process, the free deployment results in a highly dynamic response for the CTLT. As shown in Fig. 8, as soon

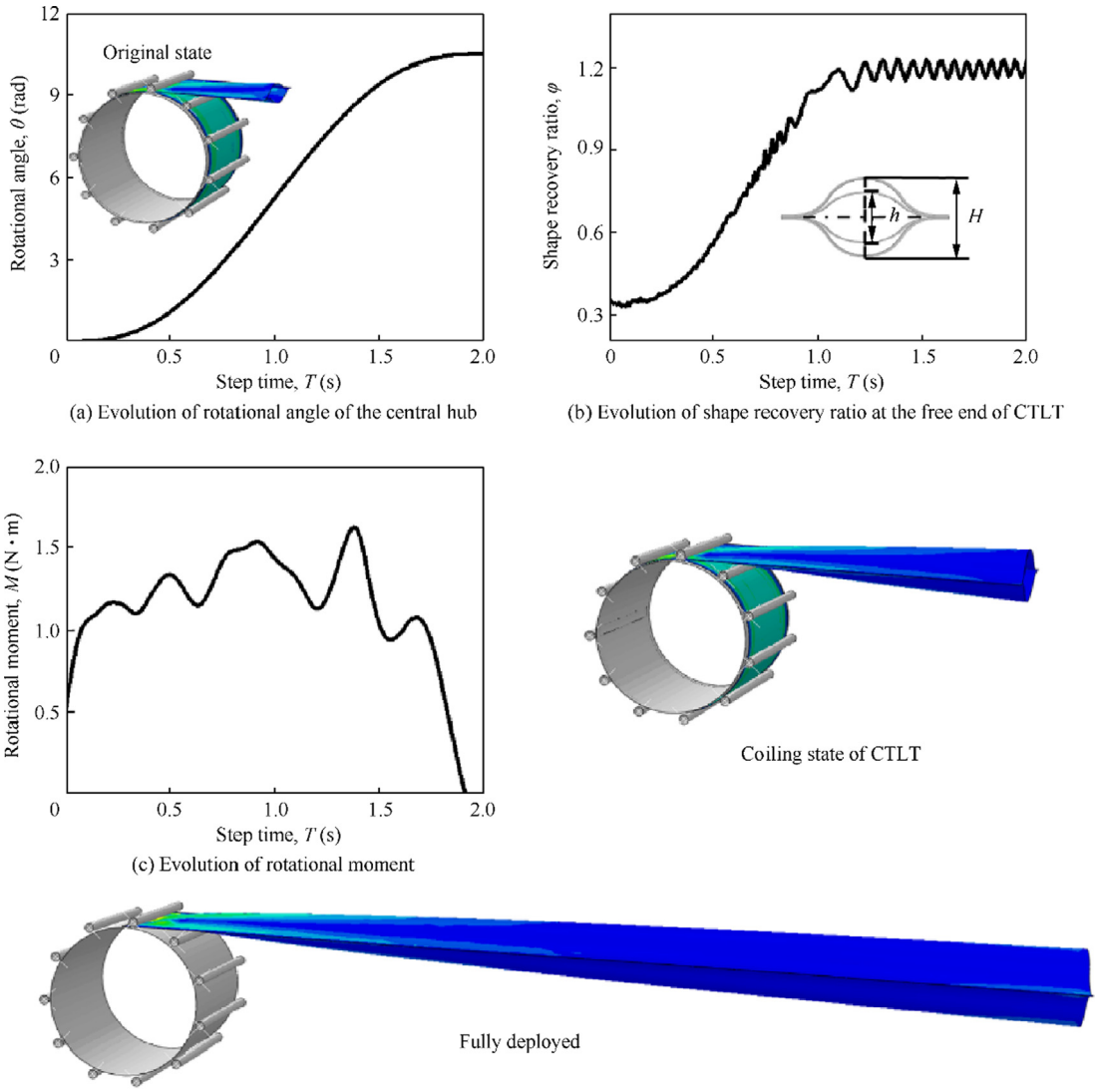

(a) Evolution of rotational angle of the central hub

(b) Evolution of shape recovery ratio at the free end of CTLT

(c) Evolution of rotational moment

(d) FEM snapshots for CTLT in the quasi-static deployment process

Fig. 7 Mechanical response of CTLT in controlled deployment process.

as the guide rollers are removed, the CTLT deploys dynamically with one end attached on the hub and the other end moves rapidly along a spiral trajectory. The dynamic deployment behavior of the CTLT was quantified by calculating the deployment angle α, which is defined by the included angle between the current orientation and the initial orientation for the center line of the CTLT as illustrated in Fig. 8(d). The deployment angle α is plotted as a function of the step time in Fig. 8(a), which demonstrates that the CTLT deploys to its fully deployed state in less than 1 second as soon as the guide rollers are removed. Fig. 8(b) shows that the cross-section of the free end opens up rapidly in about 0.1 s, and then stabilizes at a level of $\approx$1.2; the noise in the numerical simulation corresponds to vibrations that exist in the process. Fig. 8(c) gives the normal reaction force acting on the constraint plate in the free deployment process. We note that the dynamic deployment behavior of the CTLT in the free deployment process is highly affected by the damping used in the simulation. The coefficient for the viscous pressure damping is set to 1.0×10^{-8} to damp out unwanted vibrations. A larger damping coefficient results in decreasing the deployment speed and increasing the time spent for reaching the fully deployed state, while a smaller damping coefficient may lead to overshooting and oscillations.[33,40] Only one single CTLT was modeled in this study for a detailed analysis of its coiling and deployment behaviors. However, an important point is that in actual engineering practice, CTLTs are regularly used as a group of rib structures that support the deployment of membranes, and the coiling and deployment of CTLTs would be affected by the deformation of surrounding materials. A complete model consisting of numerous CTLTs and membrane reflectors are needed in future to better capture the real behavior of the system and to provide a more accurate performance analysis of the CTLT.[41–44].

Fig. 9 shows the energy balance histories of the CTLT in the throughout process of coiling and deployment. It is shown

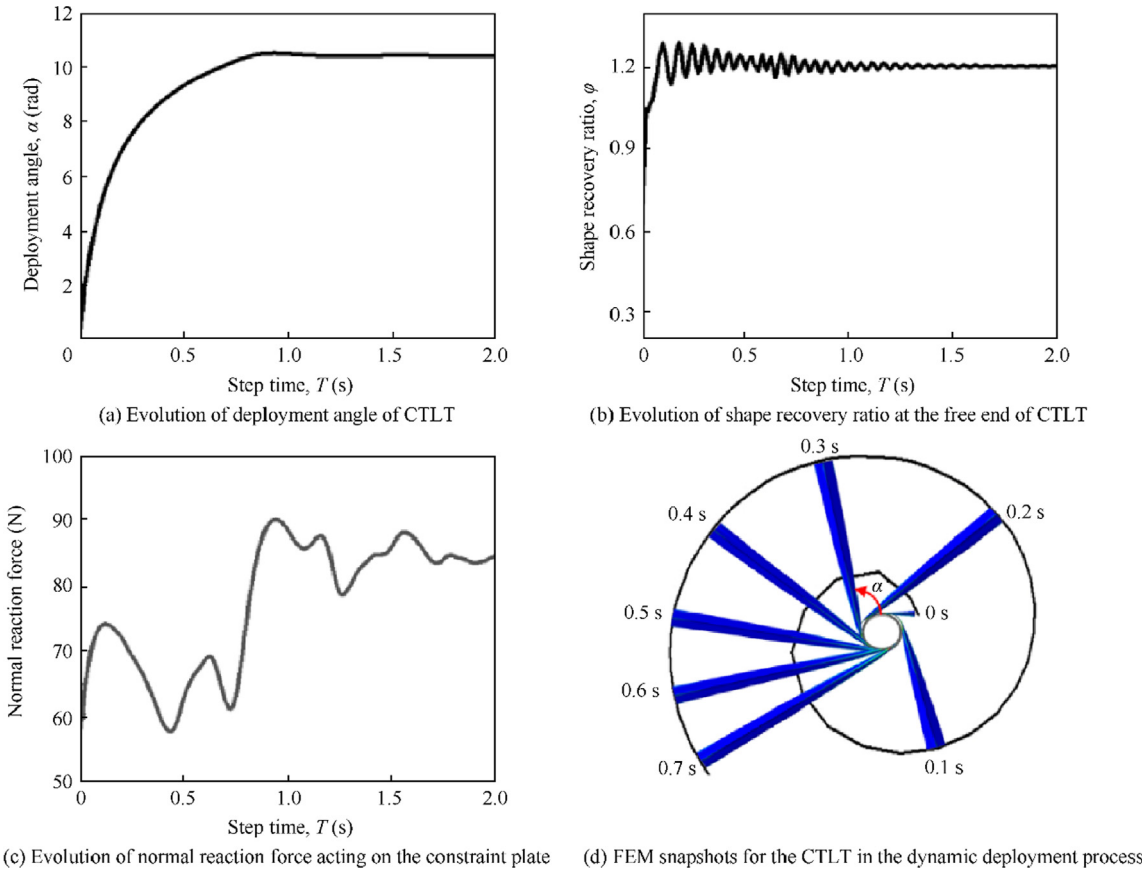

(a) Evolution of deployment angle of CTLT

(b) Evolution of shape recovery ratio at the free end of CTLT

(c) Evolution of normal reaction force acting on the constraint plate

(d) FEM snapshots for the CTLT in the dynamic deployment process

Fig. 8 Mechanical response of CTLT in free deployment process.

that the strain energy increases when the CTLT is being flattened and coiled, and is then released in the deployment process. The kinetic energy is negligible compared to the strain energy in the folding process, which indicates that all work done by external forces is stored in the elastic energy of the deformed structure. The accurate calculation of stored strain energy is critical because it provides the driving force for the subsequent deployment. An important result is that the strain energy profile is mostly symmetric for the case where the CTLT is deployed in a quasi-static controlled manner. On the contrary, the strain energy drops at a notably faster rate for the free deployment process where the kinetic energy of the CTLT is also not negligible, indicating a true dynamic process. Finally, the strain energy at the end of the deployment remains a constant ~ 2.3 J, approximately equals to that for the fully flattened state before coiling. This is because the end of the CTLT is stilled flattened and attached to the central hub at the final state.

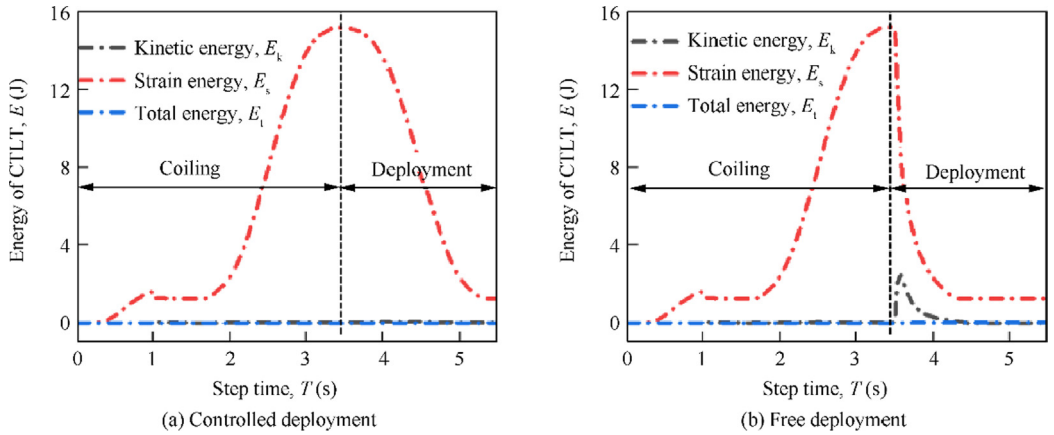

(a) Controlled deployment

(b) Free deployment

Fig. 9 Variation of strain energy of CTLT in (a) controlled deployment and (b) free deployment process.

Table 3 Prony series coefficients for PMT-F4 epoxy matrix at reference temperature $T_0 = 40^\circ C$.

i	∞	1	2	3	4	5	6	7
E_m^i (MPa)	1000	224.1	450.8	406.1	392.7	810.4	203.7	1486.0
τ_i (s)		1.0×10^3	1.0×10^5	1.0×10^6	1.0×10^7	1.0×10^8	1.0×10^9	1.0×10^{10}

5. Effect of storage time and temperature

In this section, we move on to analyze the effect of storage time and temperature on the relaxation of the stored strain energy and the deployment behavior of CTLT. To begin with, the effective material properties of T300/PMT-F4 unidirectional lamina at the initial state and after being stowed at a variety of temperature and time scales were calculated from constituent fiber and matrix properties. The fiber volume fraction in each lamina is chosen to be $V_f = 0.4$, and the fiber and matrix properties are obtained from experiments.[30] T300 carbon fiber is assumed as linear elastic and transversely isotropic with properties $E_1 = 233\text{GPa}$, $E_2 = 15\text{GPa}$, $v_{12} = 0.2$, $v_{23} = 0.33$, $G_{12} = 8.963\text{GPa}$. The PMT-F4 epoxy matrix is assumed as isotropic and linear viscoelastic, and the modulus relaxation is defined by generalized Maxwell model with Prony series expressed as:

$$E(t) = E_0 - \sum_{i=1}^{n} E_i e^{-\frac{t}{\tau_i \alpha_T}} \tag{2}$$

where $E(t)$ denotes the matrix modulus as function of storage time. E_0 is the instantaneous modulus, and E_i and τ_i are the modulus and relaxation time constant of the i-th arm of the generalized Maxwell model. Eq. (2) indicates that the modulus of epoxy decreases with time from the initial value E_0 to the long-term modulus $E_\infty = E_0 - \sum_{i=1}^{n} E_i$. The Prony series coefficients at the reference temperature $T_0 = 40^\circ C$ are given in Table 3. Additionally, α_T is a time temperature shift factor that reflects the effect of temperature on the relaxation, which takes the Williams-Landel-Ferry (WLF) form:

$$\lg(\alpha_T) = -\frac{C_1(T - T_0)}{C_2 + (T - T_0)} \tag{3}$$

where T_0 is the reference temperature at which the relaxation data is given, T is the temperature of interest, and $C_1 = 28.3816$ and $C_2 = 93.291$ are the calibration constants at the reference temperature.

Taking the known properties of fiber and matrix as inputs, the effective material properties of T300/PMT-F4 unidirectional lamina at the initial state and after being stowed for 1 month, 1 year, and 2 years under a variety of temperatures at 30 ℃, 40 ℃, and 50 ℃ were calculated by performing a series of FE-RVE analyses using the open-source ABAQUS plug-in Viscoelastic RVE Calculator.[45] The results are summarized in Table 4, which show that the elastic modulus of the lamina decreases with storage time, and decreases even faster at a higher temperature than at a lower temperature.

Then, deployment simulations were carried out with the above relaxed material properties of composites. The simulation setup is almost the same as described in Section 2, except that the lamina properties shall be updated to new values before conducting the deployment analysis, so as to incorporate the influence of change in material properties during stowage. The desired update is achieved by using a virtual temperature technique, where each set of lamina properties is related to a distinct virtual temperature, and the change in virtual temperature gives rise to the update of material properties from the originally unrelaxed state to a relaxed state. More details about this method could be found in a previous study.[45] Moreover, to accentuate the influence of stress relaxation in this particular example, a CTLT boom with a length of 2.0 m was modeled. This longer length enabled it to be coiled around the central hub nearly six circles.

Fig. 10(a) compares deployment time for CTLT that has been stored for 1 month, 1 year and 2 years at three different temperature levels 30 ℃, 40 ℃ and 50 ℃. It can be seen that the deployment of CTLT becomes slower because it takes longer time for deployment after being stored for a longer time at a higher temperature. These results are consistent with the experimental observations reported by Adamcik et al.[29] and could be explained by the decrease in the stored strain energy of the folded boom during storage, as shown in Fig. 10(b). Specifically, the stored stain energy decreases with storage time and decreases more rapidly at a higher temperature than a lower temperature. The results shown in Fig. 10 also indicate that

Table 4 Lamina properties of T300/PMT-F4 after relaxation at different storage time and temperature levels.

Mechanical Property	Initial state	Storage temperature is 30℃			Storage temperature is 40℃			Storage temperature is 50℃		
		1 month	1 year	2 years	1 month	1 year	2 years	1 month	1 year	2 years
E_1(GPa)	96.21	96.12	96.04	96.01	95.50	95.19	95.07	94.61	93.96	93.83
E_2(GPa)	7.85	7.68	7.52	7.46	6.45	5.76	5.50	4.38	2.57	2.18
v_{12}	0.27	0.27	0.27	0.27	0.27	0.27	0.27	0.27	0.27	0.27
G_{12}(GPa)	0.43	0.43	0.43	0.43	0.44	0.44	0.44	0.44	0.45	0.45
G_{23}(GPa)	3.20	3.13	3.06	3.03	2.60	2.31	2.20	1.74	1.00	0.85

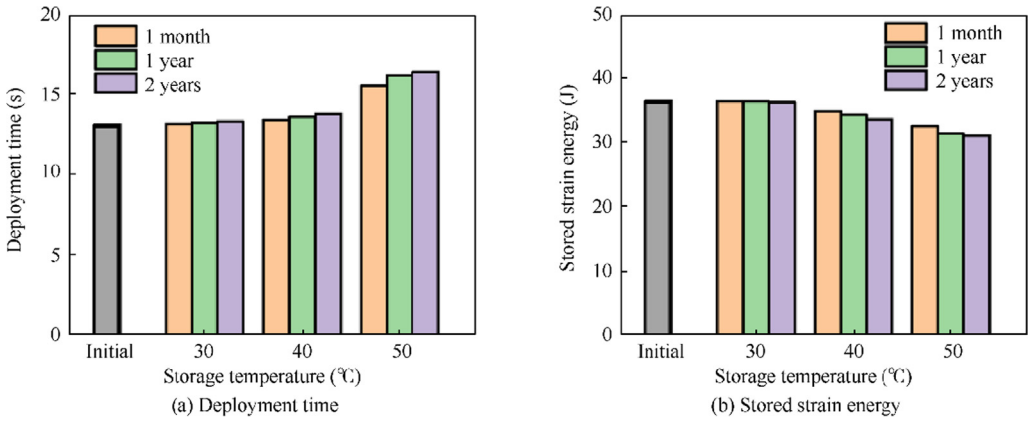

Fig. 10 Effect of storage time and temperature on performance of CTLT.

storage temperature has a much more significant effect on the deployment performance than storage time.

6. Concluding remarks

CTLT has been proposed as one of the most promising candidates for the design of various deployable space structures. A comprehensive analysis of the behavior of coiling and deployment is crucial for understanding the performance of CTLT. The physically experimental test of the deployment of CTLT could be time-consuming and costly due to the requirement of gravity-unloading mechanisms for simulating the microgravity environment in space. As a result, numerical simulation provides a cost-effective alternative approach. However, it is also challenging to develop a reliable numerical model to accurately predict the mechanical behaviors of CTLT throughout the complete process of flattening, coiling, storage and deployment, because these processes are involved with complex deformations such as unstable behaviors, complicated contacts and interactions between deformable CTLT and rigid objects.

Based on finite element method, this paper describes a computational strategy for the coiling and deployment analysis of CTLT, considering both deformable CTLT and rigid-bodies mechanisms, including the central hub and guide rollers, as well as the complex interactions among them. The behavior of CTLT in flattening and coiling process was firstly simulated using a quasi-static method. The evolution of strain energy stored in the deformation of CTLT was obtained, and the rotational moment required to rotate the central hub was predicted. The results show a good agreement with experimental data in literature. Then, on the basis of the coiled and stowed results, both the quasi-static controlled deployment and the dynamic free deployment behaviors of CTLT were simulated and compared. The release of the stored strain energy was captured, and the deployment speed was predicted. Finally, the storage of the CTLT at an elevated temperature significantly affects the dynamic deployment. The simulation results show that the deployment speed of CTLT decreases when it has been stored in a higher temperature environment for an extended period.

The simulation results demonstrate the capability of the proposed simulation techniques. The numerical strategy proposed here is readily applicable to the coiling and deployment analysis of other thin-walled booms made from metallics and/or composites, such as the C-shaped tape springs, Storable Tubular Extensible Mast (STEM) booms, and Triangular Rollable And Collapsible (TRAC) booms. We have made the source Python scripts publicly available for reproducing the FEM model and simulations in this manuscript. We hope our efforts contribute to improving understanding of the coiling and deployment performance of CTLT, and provide helpful numerical studies and FEM codes for the community.

Declaration of Competing Interest

The authors declare that they have no known competing financial interests or personal relationships that could have appeared to influence the work reported in this paper.

Acknowledgements

This research was co-supported by the National Natural Science Foundation of China (No.12202295), the Fundamental Research Funds for the Central Universities, China (No. YJ2021137), the Open Project of State Key Laboratory for Strength and Vibration of Mechanical Structures, Xi'an Jiaotong University, China (No. SV2021-KF-04), and the Open Project of State Key Laboratory of Structural Analysis for Industrial Equipment, Dalian University of Technology, China (No. GZ22120).

Appendix A. Supplementary material

Supplementary data to this article can be found online at https://doi.org/10.1016/j.cja.2023.05.011.

References

1. Fernandez JM, Rose G, Stohlman OR, et al. An advanced composites-based solar sail system for interplanetary small satellite missions.Reston: AIAA; 2018.Report No.:AIAA-2018-1437.
2. Fernández JM, Rose G, Younger CJ, et al. NASA's advanced solar sail propulsion system for low-cost deep space exploration and science missions that use high performance rollable composite booms. 2017.

3. Yoshiro O, Reveles J, Fraux V,et al.Deployable wrapped rib assembly. United States patent US WO2018087541A1. 2019 Nov 28.
4. Ma XF, Li TJ, Ma JY, et al. Recent advances in space-deployable structures in China. *Engineering* 2022;**17**:207–19.
5. Liu JG, Zhao PY, Wu CC, et al. SIASAIL-I solar sail: from system design to on-orbit demonstration mission. *Acta Astronaut* 2022;**192**:133–42.
6. Zhao PY, Wu CC, Li YM. Design and application of solar sailing: a review on key technologies. *Chin J Aeronaut* 2023;**36**(5):125–44.
7. Xue ZH, Liu JG, Wu CC, et al. Review of in-space assembly technologies. *Chin J Aeronaut* 2021;**34**(11):21–47.
8. Dong KJ, Li DL, Lin QH, et al. Design and analysis of a novel hinged boom based on cable drive. *Chin J Aeronaut* 2022;**35**(3):592–606.
9. Xiong JJ, Shenoi RA. General aspects on structural integrity. *Chin J Aeronaut* 2019;**32**(1):114–32.
10. Fernandez JM. Advanced deployable shell-based composite booms for small satellite structural applications including solar sails. *Int Sympos Sol Sail* 2017.
11. Jia QL, An N, Ma XF, et al. Exploring the design space for nonlinear buckling of composite thin-walled lenticular tubes under pure bending. *Int J Mech Sci* 2021;**207** 106661.
12. Yang H, Fan SS, Wang Y, et al. Novel four-cell lenticular honeycomb deployable boom with enhanced stiffness. *Materials (Basel)* 2022;**15**(1):306.
13. Bai JB, Chen D, Xiong JJ, et al. A corrugated flexible composite skin for morphing applications. *Compos B Eng* 2017;**131**:134–43.
14. Fernandez JM, Volle CE. *Corrugated rollable tubular booms*. Reston: AIAA; 2021, Report No.:AIAA-2021-0296.
15. Wu Z, Xiang P, Wu M,et al. Design, analysis and testing of a 0.5 m diameter wrapped rib-tensioned surface reflector demonstrator. *Proceedings of IASS annual symposia, Vol. 2018, International association for shell and spatial structures (IASS)*. 2018.
16. Chen WJ, Fang GQ, Hu Y. An experimental and numerical study of flattening and wrapping process of deployable composite thin-walled lenticular tubes. *Thin Walled Struct* 2017;**111**:38–47.
17. Bai JB, Chen D, Xiong JJ, et al. Folding analysis for thin-walled deployable composite boom. *Acta Astronaut* 2019;**159**:622–36.
18. Chu ZY, Lei YA. Design theory and dynamic analysis of a deployable boom. *Mech Mach Theory* 2014;**71**:126–41.
19. Firth JA, Pankow MR. Minimal unpowered strain-energy deployment mechanism for rollable spacecraft booms: ground test. *J Spacecr Rockets* 2019;**57**(2):346–53.
20. Liu TW, Bai JB, Fantuzzi N. Folding behavior of the thin-walled lenticular deployable composite boom: Analytical analysis and many-objective optimization. *Mech Adv Mater Struct* 2022:1–19.
21. Long YF, Garaizar OR, Fernandez JM, et al. *Multiscale simulation of deployable composite structures*. Reston: AIAA; 2021, Report No.:AIAA-2021-0199.
22. Leclerc C, Wilson LL, Bessa MA, et al. *Characterization of ultra-thin composite triangular rollable and collapsible booms*. Reston: AIAA; 2017, Report No.:AIAA-2017-0172.
23. Stabile A, Laurenzi S. Coiling dynamic analysis of thin-walled composite deployable boom. *Compos Struct* 2014;**113**:429–36.
24. Jin H, Jia QL, An N, et al. Surrogate modeling accelerated shape optimization of deployable composite tape-spring hinges. *AIAA J* 2022;**60**(10):5942–53.
25. Yang H, Guo HW, Liu RQ, et al. Coiling and deploying dynamic optimization of a C-cross section thin-walled composite deployable boom. *Struct Multidiscip Optim* 2020;**61**(4):1731–8.
26. Zhang Z, Zhou HP, Ma JY, et al. Space deployable bistable composite structures with C-cross section based on machine learning and multi-objective optimization. *Compos Struct* 2022;**297** 115983.
27. Bai JB, Xiong JJ. Temperature effect on buckling properties of ultra-thin-walled lenticular collapsible composite tube subjected to axial compression. *Chin J Aeronaut* 2014;**27**(5):1312–7.
28. Bai JB, Shenoi RA, Xiong JJ. Thermal analysis of thin-walled deployable composite boom in simulated space environment. *Compos Struct* 2017;**173**:210–8.
29. Adamcik B, Firth J, Pankow M, et al. *Impact of storage time and operational temperature on deployable composite booms*. Reston: AIAA; 2020, Report No.:AIAA-2020-1183.
30. Kwok K, Pellegrino S. Micromechanics models for viscoelastic plain-weave composite tape springs. *AIAA J* 2016;**55**(1):309–21.
31. Long YF, Rique O, Fernandez JM, et al. Simulation of the column bending test using an anisotropic viscoelastic shell model. *Compos Struct* 2022;**288** 115376.
32. Mallikarachchi HMYC, Pellegrino S. Quasi-static folding and deployment of ultrathin composite tape-spring hinges. *J Spacecr Rockets* 2011;**48**(1):187–98.
33. Mallikarachchi HMYC, Pellegrino S. Deployment dynamics of ultrathin composite booms with tape-spring hinges. *J Spacecr Rockets* 2014;**51**(2):604–13.
34. Jia QL, An N, Ma XF, et al. A dynamic finite element procedure for bending collapse of composite thin-walled lenticular tubes. *Compos Struct* 2022;**287** 115364.
35. Lee AJ, Fernandez JM, Daye JG. *Bistable deployable composite booms with parabolic cross-sections*. Reston: AIAA; 2022, Report No.:AIAA-2022-2264.
36. Wang LW, Bai JB, Shi Y. Simplified analytical model for predicting neutral cross-section position of lenticular deployable composite boom in tensile deformation. *Materials (Basel)* 2021;**14**(24):7809.
37. Hoskin A, Viquerat A, Aglietti GS. Tip force during blossoming of coiled deployable booms. *Int J Solids Struct* 2017;**118–119**:58–69.
38. Wang SC, Schenk M, Jiang SY, et al. Blossoming analysis of composite deployable booms. *Thin Walled Struct* 2020;**157** 107098.
39. Wang SC, Schenk M, Guo HW, et al. Tip force and pressure distribution analysis of a deployable boom during blossoming. *Int J Solids Struct* 2020;**193–194**:141–51.
40. Soykasap Ö. Deployment analysis of a self-deployable composite boom. *Compos Struct* 2009;**89**(3):374–81.
41. Morozov EV, Lopatin AV, Khakhlenkova AA. Finite-element modelling, analysis and design of anisogrid composite lattice spoke of an umbrella-type deployable reflector of space antenna. *Compos Struct* 2022;**286** 115323.
42. Klimm W, Kwok K. *Surface accuracy of viscoelastic composite thin-shell deployable reflector antennas*. Reston: AIAA; 2020, Report No.:AIAA-2020-0932.
43. Lim JH, Kim YB, Jang IS, et al. Parabolic deployable mesh antenna with a hingeless system of superelastic SMA ribs and composite tape springs. *Acta Astronaut* 2022;**200**:149–62.
44. Wu D, Wu ME, Xiang P, et al. Surface accuracy analysis and optimization design of rib-mesh paraboloidal antenna reflectors. *Aerosp Sci Technol* 2022;**129** 107817.
45. An N, Jia QL, Jin H, et al. Multiscale modeling of viscoelastic behavior of unidirectional composite laminates and deployable structures. *Mater Des* 2022;**219** 110754.